Preprint Title	Mechanochemical bottom-up synthesis of phosphorus-linked, heptazine-based carbon nitrides using sodium phosphide
Authors	Blaine G. Fiss, Georgia Douglas, Michael Ferguson, Jorge Becerra, Jesus Valdez, Trong-On Do, Tomislav Friscic and Audrey H. Moores
Publication Date	07 Jun 2022
Article Type	Letter
Supporting Information File 1	ESI_g-h-PCN_BJOC2022_v4_Formatted.docx; 550.4 KB
ORCID® iDs	Blaine G. Fiss - https://orcid.org/0000-0002-4791-3689; Audrey H. Moores - https://orcid.org/0000-0003-1259-913X

Mechanochemical bottom-up synthesis of phosphorus-linked, heptazine-based carbon nitrides using sodium phosphide

Blaine G. Fiss,[1‡] Georgia Douglas,[1‡] Michael Ferguson,[1] Jorge Becerra,[2] Jesus Valdez,[3] Trong-On Do,[2*] Tomislav Friščić,[1*] Audrey Moores,[1,4*]

Address: [1]Centre in Green Chemistry and Catalysis, Department of Chemistry, McGill University, 801 Sherbrooke Street West, Montréal, Québec, Canada; [2]Department of Chemical Engineering, Laval University, Québec City, Québec, Canada; [3]Facility for Electron Microscopy Research (FEMR), McGill University, Montréal, Québec, Canada and [4]Department of Materials Engineering, McGill University, 3610 University Street, Montréal, Québec, Canada.

Email: Trong-On Do – trong-on.do@gch.ulaval.ca

Email: Tomislav Friščić – tomislav.friscic@mcgill.ca

Email: Audrey Moores – audrey.moores@mcgill.ca

* Corresponding author

‡ Equal contributors

Abstract

Herein we present the bottom-up, mechanochemical synthesis of phosphorus-bridged heptazine based carbon nitrides (g-h-PCN). The structure of these materials was determined through a combination of powder X-ray diffraction (PXRD), X-ray photoelectron spectroscopy (XPS), ^{31}P magic angle spinning nuclear magnetic resonance (MAS NMR), density functional theory (DFT) and electron energy loss spectroscopy (EELS). Compared to traditional furnace-based techniques, the presented method utilizes milder conditions, as well as shorter reaction times. Both samples of g-h-PCN directly after milling and aging and after an hour of annealing at 300 °C (g-h-PCN300) show a reduction in photoluminescent recombination, as well as a nearly two-time increase in photocurrent under broad spectrum irradiation, which are appealing properties for photocatalysis.

Keywords

Introduction

The development of heteroatom-doped graphitic carbon nitrides (g-CN) has been a rapidly growing area of research since their first report towards water splitting in 2009.[1] Since that time, the addition of elements such as boron,[2] phosphorus,[3-5] sulfur and oxygen[6] have shown to help minimize the bandgap of these metal-free photocatalysts as well as improve their overall stability. Traditional routes to incorporate phosphorus have relied on high-temperature[7] or microwave[8] syntheses, and often proceed through the introduction of a phosphorus atom within the

2

heptazine ring, which constitutes the building block of g-CN, as opposed to in a linking position. Computational studies by Hartley and Martsinovich have investigated the influence of various linkers, including phosphorus atoms, on both the structure and optical behaviour of heptazine based graphitic carbon nitrides.[3] Yet, experimental examples of carbon nitrides linked together *via* phosphorus atoms are limited, likely due to challenges in controlling the insertion of phosphorus as linkers under high energy conditions. Mechanochemistry[9-12] has proven to be effective for the synthesis of a variety of polymers,[13-17] nanomaterials,[18-22] crystal engineering[23-25] as well as inorganic[26-30] and organic small molecules.[31-37] The removal of bulk solvent and mild reaction conditions allowed by such techniques are not only beneficial from a green chemistry perspective,[11] but they also afford conditions conducive to new reactivities and the development of novel materials.[9] In earlier works from our group, we have explored the synthesis of phosphorus-bridged g-CN type materials produced from a triazine unit and found that the material hence produced featured good photochemical properties (Scheme 1).[38] Yet conventional g-CN materials are not based of triazine units, but rather of heptazine ones, thus featuring more open structures. In an effort to replicate a structure closer to known g-CN, we explored herein the use of solvent-free, room temperature mechanochemistry to access phosphorus linked carbon nitride with repeating heptazine units, showing improved photochemistry over pristine graphitic carbon nitride (g-CN). Additionally, the effect of a 1 h anneal on the overall structure and photochemical properties was investigated at 300 °C.

Results and Discussion

Employing a similar method to one previously developed by our group (Scheme 1a),[38] equimolar amounts of sodium phosphide and trichloroheptazine were combined in a vibrational ball mill and milled at 30 Hz for 90 min under an argon atmosphere (Scheme 1b). As trichloroheptazine was not readily available commercially, it was synthesized from melem in three steps following a known procedure (see SI for detailed procedure).[4] The milled powder was then allowed to age under an argon atmosphere for 24 h, prior to washing via centrifugation in a 3:1 volume mixture of ethanol and deionized (DI) water. This afforded a material referred to below as g-h-PCN. Alternative, the sample was annealing for 1 h anneal at 300 °C under a flow of argon gas, affording g-h-PCN300.
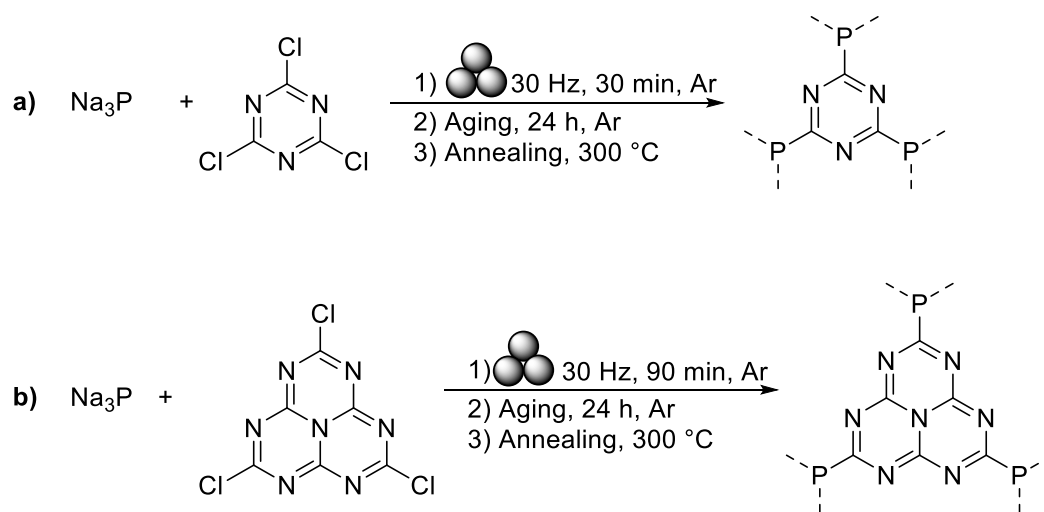
Scheme 1: a) Mechanochemical synthesis of g-PCN from sodium phosphide and trichlorotriazine (previous work[38]) and b) g-h-PCN from sodium phosphide and trichloroheptazine (this work).

Powder X-ray diffraction (PXRD)

To confirm the formation of a layered structure, powder X-ray diffraction (PXRD) was performed on g-h-PCN and g-h-PCN300 (Figure 1, green and teal). Both g-h-PCN and

g-h-PCN300 were largely amorphous but showed two broad Bragg reflections at 2θ =16 ° and 2θ = 28 °. This suggests the high thermal stability of the g-h-PCN structure, being readily formed during the mild milling and aging conditions, with no need for annealing.
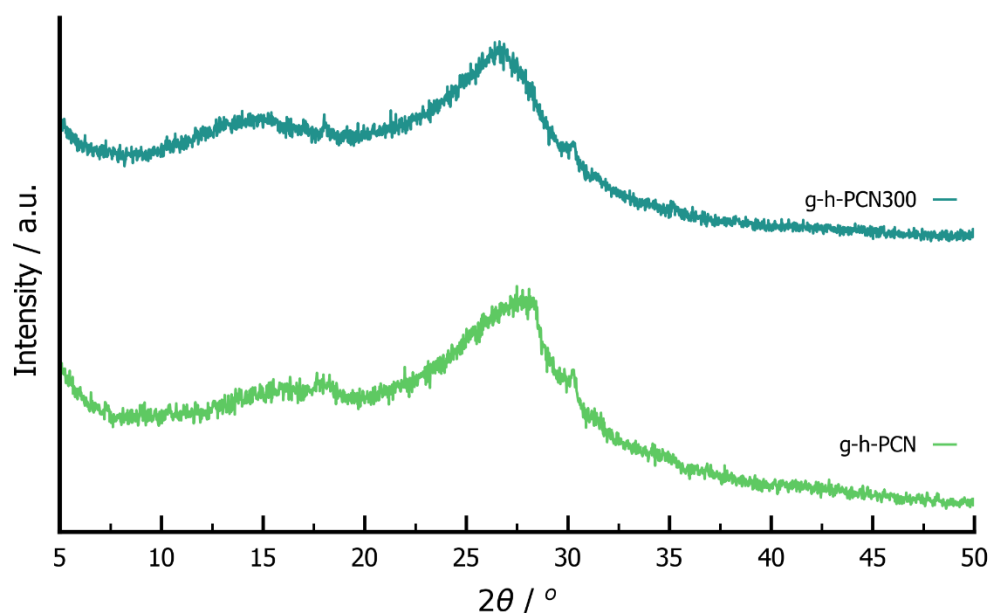

Figure 1: PXRD patterns of g-h-PCN (green) and g-h-PCN300 (teal).

X-ray photoelectron spectroscopy (XPS)

To gain insight into the atomic speciation within the structure and establish phosphorus atoms are linkers between heptazine units, X-ray photoelectron spectroscopy (XPS), was used to probe the surface. In g-h-PCN, XPS scans focused on carbon 1s showed three major peaks at 284.7, 286.4, and 288.6 eV, corresponding to C=N, C-OH and C=O signals, respectively (Figure 2a), as well as a peak centered on 292.1 eV due to charging effects.[39] The presence of C=N bonds established by XPS indicates that the heptazine structure was preserved during milling and aging with Na_3P. Nitrogen 1s focused scans of g-h-PCN show a 62% to 38% ratio of pyridinic to pyrrolic/pyridonic-N type nitrogen environments, centred on 399.0 eV and 400.7 eV respectively[40, 41] (Figure 2b). This suggests that while the majority of the heptazine ring remained

pyridinic in nature, partial reduction of the ring structure, due to the reductive nature of Na₃P and mild oxidation during ambient workup following milling and aging, can also have occurred. Additionally, the phosphorus 2p signal in g-h-PCN showed the majority of phosphorus exists as a mixture of P=O and P-O species, with a major peak centred at 133.6 eV (69%, Figure 2c). These species are formed by oxidation with air and hydrolysis upon quenching in water and ethanol at the end of the aging step. g-h-PCN300 features the same three major carbon 1s peaks at 284.8, 286.2 and 288.2 eV for C=N/C=C, C=O and C-OH species respectively, as well as the charging peak seen in g-h-PCN. In g-h-PCN300, a reduction of the C=N ratio to 37%, reduction of C=O character from 21% to 18% compared to g-h-PCN and an increase in C-OH character from 35% to 43% suggests mild hydrolysis, likely of terminal chloroheptazine, during the anneal at 300 °C, even under a flow of argon gas. (Figure 2d). The nitrogen 1s scans show a similar trend, with the ratio of pyridinic and pyrrolic/pyridone nitrogen being 68% and 29%, respectively, compared to 62% and 28% in g-h-PCN. (Figure 2e). Phosphorus 2p focused scans of g-h-PCN300 show a slight reduction in P-O and P=O bond character from g-h-PCN to g-h-PCN300 down from 69% to 66% Figure 2f).
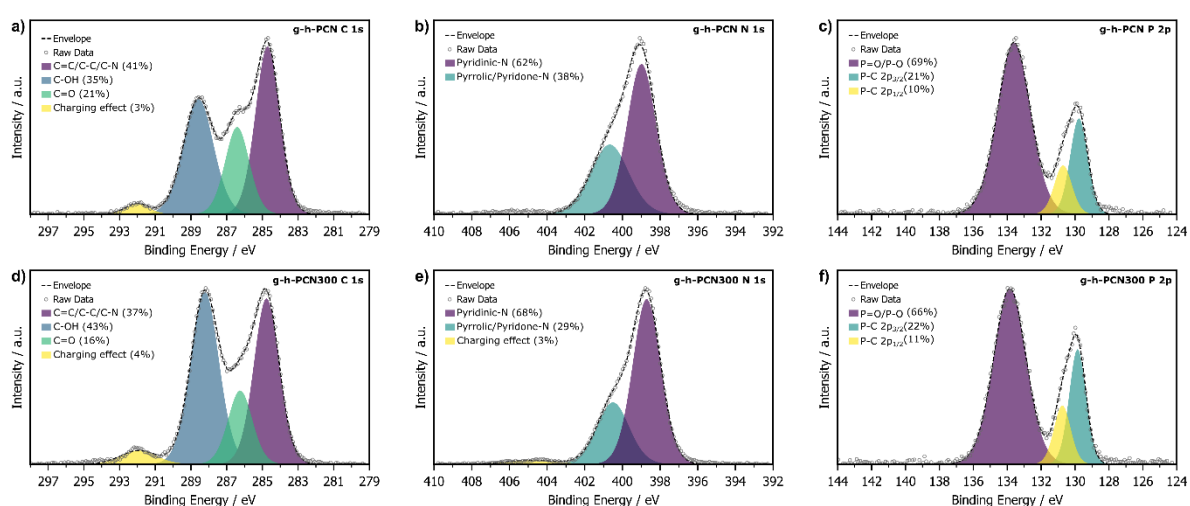
Figure 2: XPS scans of a) C 1s b) N 1s and c) P 2p for the pre-annealed g-h-PCN and d) C 1s e) N 1s and f) P 2p focused scans of g-h-PCN300 after annealing at 300 °C for 1 h.

FTIR-ATR analysis

The structural motifs seen through XPS were further supported by FTIR-ATR spectra. For g-h-PCN, the sharp peak at 800 cm^{-1} was indicative of the heptazine breathing mode, typically seen for C_3N_4 materials.[42] C=N and bond retention was also further supported by a series of peaks in the range of 1300-1800 cm^{-1}. While retention of the heptazine ring structure was shown by FTIR, a small, additional peak at ~950 cm^{-1} is also seen, indicative of the formation of a P-C bond,[43] supporting the results seen from previously discussed XPS data (Figure S3, green). In g-h-PCN300, the structure showed similar features to g-h-PCN, retaining the sharp peak corresponding to the heptazine breathing mode at 800 cm^{-1}, while also retaining the P-C vibration at 950 cm^{-1} (Figure S3, teal).

STEM-EELS analysis

The composition and particle morphology were investigated further using scanning tunneling electron microscopy-electron energy loss spectroscopy (STEM-EELS).The g-h-PCN sample prior to annealing showed equal distribution of carbon and nitrogen with minimal phosphorus present, with particles roughly 400 nm in length (Figure S4a). Upon annealing at 300 °C for 1 h under argon, the phosphorus content is shown to increase, while still remaining partially localized, with the particles retaining their size and morphology (Figure S4b).

7

[31]P magic angle spinning (MAS) NMR

Bulk solid-state analysis of the heptazine-based materials showed similar resonances to previous work by our group on phosphorus-linked triazine networks.[38] The ^{31}P MAS NMR of g-h-PCN showed a broad resonance centered around -8.9 ppm, with a sharp residual phosphate resonance at 0.9 ppm (Figure 2a). NMR analysis of similar materials, both by our group and others suggest that the broad resonance corresponds to a largely amorphous phase with predominately phosphate and phosphite-like environments, with the broad at -8.9 ppm possibly corresponding to hydrated sodium phosphate byproducts.[44, 45] g-h-PCN300 on the other end showed an up-field shift of all main resonances toward -14.4 ppm and -20.6 ppm respectively (Figure 3b). As previously shown by our group,[38] this shift in main resonance is indicative of organization of the formed sheets, leading to a layered structure.
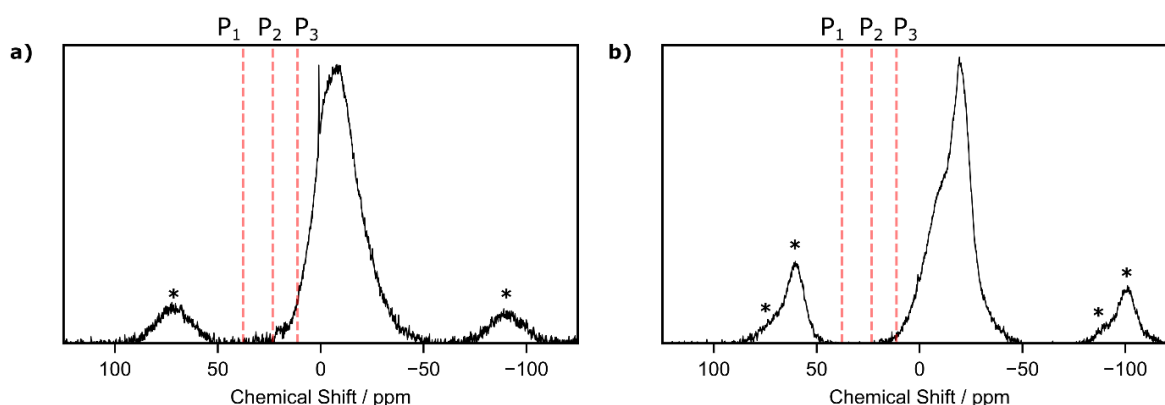

Figure 3: ^{31}P MAS NMR of a) g-h-PCN and b) g-h-PCN300. Asterisks denote spinning sidebands.

Computational analysis

The ^{31}P NMR chemical shifts were calculated using the plane wave DFT code CASTEP v20.11 (see SI for full computational details).[46] In the absence of an experimentally resolved crystal structure for g-h-PCN, we followed a similar methodology to our previous work[38] of substituting bridging nitrogen atoms for phosphorus in previously

reported heptazine-based graphitic carbon nitrides. We adapted the *ab initio* predicted structures for a networks of corrugated sheets[47] (Figure 4a and 4b) and planar sheets (Figure 4c).[48] Additionally, we modelled a chlorine terminated monomeric unit based on an experimentally resolved, nitrogen-bridged, paddlewheel structure (Figure 4d).[49] Calculations resulted in a single chemical environment for the phosphorus atoms in the three model structures. The corrugated and planar network structures have calculated ^{31}P chemical shifts at 37.7 ppm (P_1) and 23.3 ppm (P_2), respectively, while that of the paddlewheel monomer is at 11.2 ppm (P_3). These calculated shifts demonstrate that the experimental phosphorus environments are unique from those previously reported, suggesting that the mechanochemically synthesised material presented herein has a different network structure to those predicted by *ab initio* studies.[47,48]
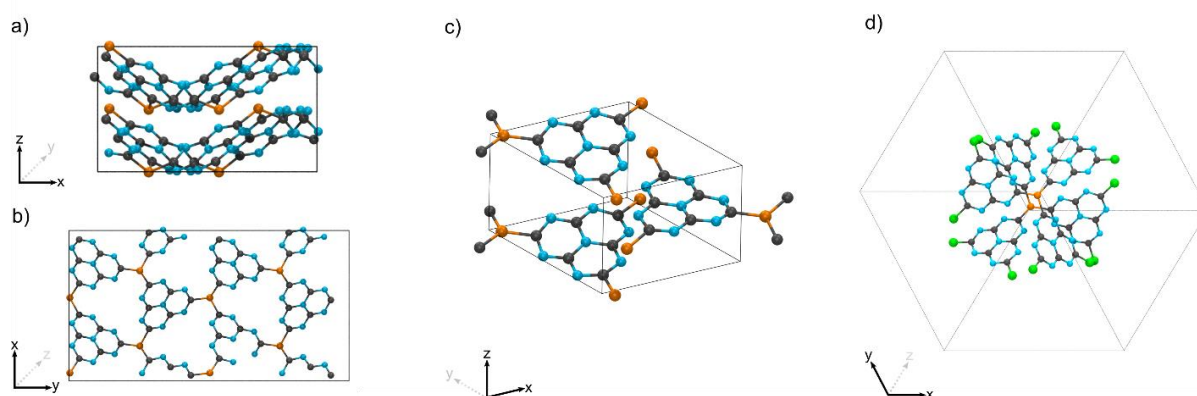

Figure 4: Calculated structures for a) corrugated (edge facing), b) corrugated (single layer), c) layered g-h-PCN and d) phosphine paddlewheel.

Photochemical behaviour

Diffuse reflectance spectroscopy (DRS) of both g-h-PCN (Figure S5a, blue trace) and g-h-PCN300 (Figure S5a, green) was analysed in regard to the performance of pure g-CN, made by annealing melamine in a loosely capped alumina crucible at 550 °C for 4 h with a ramp rate of 5 °C/min .[50] The g-CN shows an absorption edge at ~425 nm

(Figure S5a, purple trace), typical for polymerized and graphitic heptazine materials.[51,52] Both phosphorus containing structures featured broadened absorption ranges compared to g-CN, with g-h-PCN showing a redshifted maxima at ~572 nm and g-h-PCN300 showing a similar red shifted maxima at 525 nm. Additionally, photoluminescence (PL) measurements showed an initially reduced absorption intensity for g-h-PCN (Figure S5b, blue) compared to that of g-CN (Figure S5b, purple) with further reduction in absorption for g-h-PCN300 (Figure S5b, green). This reduction in photoluminescence has previously been reported for phosphorus-doped carbons and carbon nitrides,[53] as the addition of Lewis basic heteroatoms improves the stability of excitons, slowing the rate of recombination. Time-resolved lifetimes showed an increase upon replacement of the nitrogen linker for phosphorus. Nitrogen-linked g-CN showed exciton lifetimes of 4.2 μs, while the introduction of a phosphorus linker in g-h-PCN increases the lifetime to 67 μs, with g-h-PCN300 showing lifetimes of 42 μs. We have also observed a similar effect in triazine based phosphorus-linked graphitic CN structures, with lifetimes of 4.7 and 39 μs seen for g-PCN and g-PCN300 respectively.[38]

Improved charge transfer was further confirmed through photocurrent and Nyquist measurements, comparing to pristine g-CN. Photocurrent measurements showed an increase from ~3.7 to 7. μA for g-h-PCN (Figure S4c, blue) compared to pristine g-CN (Figure S4c, purple) respectively after 250 s. The g-h-PCN300 showed similar photocurrent behaviour to g-h-PCN, with photocurrent values of ~7 μA (Figure S4c, green), further demonstrating the benefit of phosphorus linkages for photoactivity. Finally, Nyquist plots of g-h-PCN (Figure S4d, blue) and g-h-PCN300 (Figure S4d, green) showed lower resistivity compared to pure g-CN (Figure S4d, purple), further supporting the idea that the g-h-PCN series enables better charge mobility in due to phosphorus linkages.

Conclusion

Mechanochemistry provides a modular, room temperature access to phosphorus-linked carbon nitrides based on heptazine units, through the combination of sodium phosphide and trichloroheptazine. A combination of PXRD, XPS, MAS NMR and DFT confirmed the formation of P-C linkages between repeating heptazine units, with retained structure. The introduction of phosphorus linkages compared to nitrogen-linked, pure g-CN showed improved photochemical behaviour, with a reduction in photoluminescent recombination, as well as exciton lifetimes increased by an order of magnitude. Overall, this supports future investigations into the room-temperature mechanochemical synthesis of heteroatom containing carbons as well as the benefit of pairing DFT calculations to experimental, structural studies.

Acknowledgements

References

1. Wang, X.; Maeda, K.; Thomas, A.; Takanabe, K.; Xin, G.; Carlsson, J. M.; Domen, K.; Antonietti, M. *Nat. Mater.* **2009**, *8* (1), 76-80.
2. Guo, Y.; Wang, R.; Wang, P.; Rao, L.; Wang, C. *ACS Sustainable Chem. Eng.* **2019**, *7* (6), 5727-5741.
3. Hartley, G. O.; Martsinovich, N. *Faraday Discuss.* **2021**, *227*, 341-358.
4. Kroke, E.; Schwarz, M.; Horath-Bordon, E.; Kroll, P.; Noll, B.; Norman, A. D. *New J. Chem.* **2002**, *26* (5), 508-512.
5. Zhang, Y.; Mori, T.; Ye, J.; Antonietti, M. *J. Am. Chem. Soc.* **2010**, *132* (18), 6294-5.
6. Liu, M.; Yang, K.; Li, Z.; Fan, E.; Fu, H.; Zhang, L.; Zhang, Y.; Zheng, Z. *Chem. Commun.* **2022**, *58* (1), 92-95.
7. Wang, Q.; Gou, H.; Zhu, L.; Huang, H.-T.; Biswas, A.; Chaloux, B. L.; Epshteyn, A.; Yesinowski, J. P.; Liu, Z.; Cody, G.; Ma, M.; Zhao, Z.; Fei, Y.; Prescher, C.; Greenberg, E.; Prakapenka, V. B.; Strobel, T. A. *ACS Mater. Lett.* **2019**, *1* (1), 14-19.
8. Zou, J.; Yu, Y.; Qiao, K.; Wu, S.; Yan, W.; Cheng, S.; Jiang, N.; Wang, J. *J. Mater. Sci.* **2020**, *55* (28), 13618-13633.
9. Do, J. L.; Friščić, T. *ACS Cent. Sci.* **2017**, *3* (1), 13-19.
10. Friščić, T.; Mottillo, C.; Titi, H. M. *Angew. Chem. Int. Ed.* **2020**, *59* (3), 1018-1029.
11. Ardila-Fierro, K. J.; Hernández, J. G. *ChemSusChem* **2021**, *14* (10), 2145-2162.
12. James, S. L.; Adams, C. J.; Bolm, C.; Braga, D.; Collier, P.; Friščić, T.; Grepioni, F.; Harris, K. D.; Hyett, G.; Jones, W.; Krebs, A.; Mack, J.; Maini, L.; Orpen, A. G.; Parkin, I. P.; Shearouse, W. C.; Steed, J. W.; Waddell, D. C. *Chem. Soc. Rev.* **2012**, *41* (1), 413-47.
13. Ohn, N.; Kim, J. G. *ACS Macro Lett.* **2018**, *7* (5), 561-565.
14. Troschke, E.; Gratz, S.; Lubken, T.; Borchardt, L. *Angew. Chem. Int. Ed.* **2017**, *56* (24), 6859-6863.
15. Casco, M. E.; Kirchhoff, S.; Leistenschneider, D.; Rauche, M.; Brunner, E.; Borchardt, L. *Nanoscale* **2019**, *11* (11), 4712-4718.
16. Schneidermann, C.; Kensy, C.; Otto, P.; Oswald, S.; Giebeler, L.; Leistenschneider, D.; Gratz, S.; Dorfler, S.; Kaskel, S.; Borchardt, L. *ChemSusChem* **2019**, *12* (1), 310-319.
17. Fiss, B. G.; Hatherly, L.; Stein, R. S.; Friščić, T.; Moores, A. *ACS Sustainable Chem. Eng.* **2019**, *7* (8), 7951-7959.
18. Moores, A. *Curr. Opin. Green Sustainable Chem.* **2018**, *12*, 33-37.
19. Rak, M. J.; Saadé, N. K.; Friščić, T.; Moores, A. *Green Chem.* **2014**, *16* (1), 86-89.
20. Malca, M. Y.; Bao, H.; Bastaille, T.; Saadé, N. K.; Kinsella, J. M.; Friščić, T.; Moores, A. *Chem. Mater.* **2017**, *29* (18), 7766-7773.
21. Xu, C.; De, S.; Balu, A. M.; Ojeda, M.; Luque, R. *Chem. Commun.* **2015**, *51* (31), 6698-713.
22. Fiss, B. G.; Vu, N. N.; Douglas, G.; Do, T. O.; Friščić, T.; Moores, A. *ACS Sustainable Chem. Eng.* **2020**, *8* (32), 12014-12024.
23. Braga, D.; Dichiarante, E.; Grepioni, F.; Lampronti, G. I.; Maini, L.; Mazzeo, P. P.; D'Agostino, S. Mechanical Preparation of Crystalline Materials. An Oxymoron? In *Supramolecular Chemistry: From Molecules to Nanomaterials*;

Steed, J. W.; Gale, P. A., Eds.; John Wiley & Sons, Ltd.: 2012; Vol. 6: Supramolecular Materials Chemistry, pp 2993-3007.

24. Toda, F.; Tanaka, K.; Sekikawa, A. *J. Chem. Soc., Chem. Commun.* **1987**, (4), 279-280.

25. Friščić, T.; Trask, A. V.; Jones, W.; Motherwell, W. D. *Angew. Chem. Int. Ed.* **2006**, *45* (45), 7546-7550.

26. Braga, D.; Giaffreda, S. L.; Grepioni, F.; Pettersen, A.; Maini, L.; Curzi, M.; Polito, M. *Dalton Trans.* **2006**, *10*, 1249-63.

27. Boldyrev, V. V.; Avvakumov, E. G. *Russ. Chem. Rev.* **1971**, *40* (10), 847.

28. Beillard, A.; Bantreil, X.; Métro, T. X.; Martinez, J.; Lamaty, F. *Chem. Rev.* **2019**, *119* (12), 7529-7609.

29. Rightmire, N. R.; Hanusa, T. P. *Dalton Trans.* **2016**, *45* (6), 2352-62.

30. Tan, D.; García, F. *Chem. Soc. Rev.* **2019**, *48* (8), 2274-2292.

31. Tanaka, K.; Toda, F. *Solvent-free organic synthesis*; Wiley Online Library: 2003; Vol. 5.

32. Wang, G. W. *Chem. Soc. Rev.* **2013**, *42* (18), 7668-700.

33. Tan, D.; Friščić, T. *Eur. J. Org. Chem.* **2018**, *2018* (1), 18-33.

34. Wang, G. W. *Chin. J. Chem.* **2021**, *39* (7), 1797-1803.

35. Zhu, S.-E.; Li, F.; Wang, G.-W. *Chem. Soc. Rev.* **2013**, *42* (18), 7535-7570.

36. Mack, J.; Fulmer, D.; Stofel, S.; Santos, N. *Green Chem.* **2007**, *9* (10), 1041-1043.

37. Fiss, B. G.; Richard, A. J.; Friščić, T.; Moores, A. *Can. J. Chem.* **2021**, *99* (2), 93-112.

38. Fiss, B. G.; Douglas, G.; Ferguson, M.; Becerra, J.; Valdez, J.; Do, T. O.; Friščić, T.; Moores, A. *ChemRxiv* **2022**.

39. Ronning, C.; Feldermann, H.; Merk, R.; Hofsäss, H.; Reinke, P.; Thiele, J. U. *Phys. Rev. B* **1998**, *58* (4), 2207-2215.

40. Schneidermann, C.; Kensy, C.; Otto, P.; Oswald, S.; Giebeler, L.; Leistenschneider, D.; Grätz, S.; Dörfler, S.; Kaskel, S.; Borchardt, L. *ChemSusChem* **2019**, *12* (1), 310-319.

41. Wang, J.; Senkovska, I.; Oschatz, M.; Lohe, M. R.; Borchardt, L.; Heerwig, A.; Liu, Q.; Kaskel, S. *J. Mater. Chem. A* **2013**, *1* (36), 10951-10961.

42. Bojdys, M. J.; Müller, J. O.; Antonietti, M.; Thomas, A. *Chem. Eur. J.* **2008**, *14* (27), 8177-8182.

43. Kumar, A.; Kumar, P.; Joshi, C.; Manchanda, M.; Boukherroub, R.; Jain, S. L. *Nanomaterials* **2016**, *6* (4), 59.

44. Turner, G. L.; Smith, K. A.; Kirkpatrick, R. J.; Oldfieldt, E. *J. Magn. Reson.* **1986**, *70* (3), 408-415.

45. MacKenzie, K. J.; Smith, M. E. Chapter 7: NMR of Other Commonly Studied Nuclei. In *Multinuclear solid-state nuclear magnetic resonance of inorganic materials*; Elsevier: New York, 2002.

46. Clark, S. J.; Segall, M. D.; Pickard, C. J.; Hasnip, P. J.; Probert, M. I. J.; Refson, K.; Payne, M. C. *Z. Kristallogr.* **2005**, *220* (5-6), 567-570.

47. Gracia, J.; Kroll, P. *J. Mater. Chem.* **2009**, *19* (19), 3013-3019.

48. Wang, J.; Hao, D.; Ye, J.; Umezawa, N. *Chem. Mater.* **2017**, *29* (7), 2694-2707.

49. Tragl, S.; Gibson, K.; Glaser, J.; Heydenrych, G.; Frenking, G.; Duppel, V.; Simon, A.; Meyer, H.-J. *Z. Anorg. Allg. Chem.* **2008**, *634* (15), 2754-2760.

50. Yan, S. C.; Li, Z. S.; Zou, Z. G. *Langmuir* **2009**, *25* (17), 10397-10401.

51. Lin, L.; Ou, H.; Zhang, Y.; Wang, X. *ACS Catal.* **2016**, *6* (6), 3921-3931.

52. Wang, Y.; Wang, X.; Antonietti, M. *Angew. Chem. Int. Ed.* **2012**, *51* (1), 68-89.

53.   Ma, X.; Lv, Y.; Xu, J.; Liu, Y.; Zhang, R.; Zhu, Y. *J. Phys. Chem. C* **2012**, *116* (44), 23485-23493.